EXAFS study of local structure at the alkali ions in superconducting K_2RbC_{60}, K_2CsC_{60}, Rb_2CsC_{60}, and Rb_3C_{60}

G. Nowitzke and G. Wortmann
Fachbereich Physik, Universität-GH Paderborn, D-33095 Paderborn, Germany

H. Werner and R. Schlögl
Fritz-Haber-Institut der Max-Planck-Gesellschaft, D-14195 Berlin-Dahlem, Germany
(Received 21 July 1995; revised manuscript received 20 May 1996)

We have studied the local site assignment as well as the structural and dynamic properties of the alkali ions in superconducting K_2RbC_{60}, K_2CsC_{60}, Rb_2CsC_{60}, and Rb_3C_{60} compounds by x-ray absorption fine structure (EXAFS) measurements at the alkali ions K, Rb, and Cs in the temperature range 14–300 K. In the ternary A_2BC_{60} systems a strong preferential site occupation is observed, where the smaller alkali ions (A) are placed in tetrahedral sites and the larger ones (B) in octahedral sites. This site ordering allows a separate structural analysis of tetrahedral and octahedral sites. A quantitative analysis of the tetrahedral site (A) dopants yields the neighbor distances $R(A\text{-}C)$, coordination numbers N_C and second cumulants σ^2. A similar analysis of the tetrahedral sites in Rb_3C_{60} was performed by creating difference spectra with the K_2RbC_{60} system. A multishell analysis of the octahedral sites (B) yields an off-center position of the B dopants. The off-center displacement scales with the size of the octahedral site and inversely with the ionic radius of the B dopant. A preferential displacement in the (1,1,1) direction is discussed in conjunction with possible carbon neighbor configurations at the octahedral sites. [S0163-1829(96)08742-5]

I. INTRODUCTION

Superconductivity in A_3C_{60} compounds is a very active field of present research and intimately connected with the structural properties.[1–7] A_3C_{60} systems with A=K, Rb show fcc structure and the space group $Fm3m$.[1,4,6] The alkali ions occupy the tetrahedral and octahedral interstitial sites in the ratio 2:1.

From the structure it is known that the octahedral sites are much larger than necessary to accommodate the respective alkali ions.[1] In contrary, the tetrahedral sites are smaller, the insertion of alkali ions such as K and Rb is accompanied by an increase of the lattice parameters a_0, reflecting the size of the respective A ion. In ternary A_2BC_{60} systems (A=K, Rb and B=Rb, Cs) the lattice constants are similarly depending on the radius of the tetrahedral site alkali ions. By choosing systems with A (B) being the smaller (larger) cation, it is expected to observe a preferential site occupation. Such a preferential site occupation has been already observed by x-ray diffraction (XRD) analysis[8,9] and NMR studies[10,11] as well as in a previous x-ray absorption study of the $K_{3-x}Rb_xC_{60}$ series by the present authors.[12] Here we present an extension of these studies to other A_2BC_{60} systems, namely K_2CsC_{60} and Rb_2CsC_{60}, where now K and Rb are expected to occupy preferentially the tetrahedral sites and Cs is expected to occupy the octahedral sites. An important point of the present study is the observation of an off-center position of the Cs ions at the octahedral site, similar to the behavior found by us for Rb in K_2RbC_{60}.[12] For this reason we present here also an improved evaluation of the data from our previous study, including the use of difference spectra to analyze separately the tetrahedral sites in Rb_3C_{60}. A short account on some aspects of this work was published in the proceedings of the XAFS-VIII conference in Berlin.[13]

In Sec. II we describe experimental details about the x-ray absorption measurements and the sample preparation. Section III presents the EXAFS data and analyses; it is divided into four sections: The raw data, the $\chi(k)$ spectra and the Fourier transforms (FT) of the respective A and B cations in the three A_2BC_{60} systems are presented in Sec. III A. The different features of the $\chi(k)$ and FT spectra of the A and B ions will give us already information about a strong preferential site occupation in these systems. Section III B will present the structural analysis of A ions located at the tetrahedral sites by applying EXAFS simulations as well as single-shell and multishell EXAFS analyses. Section III C presents the analysis of the tetrahedral sites in Rb_3C_{60} system. Section III D describes the EXAFS analysis of the B ions on the octahedral sites, where off-center positions demand for a multishell analysis. In Sec. IV the results will be discussed and compared to other EXAFS studies as well with the information obtained from other methods such as XRD and NMR.

II. EXPERIMENTAL DETAILS

We studied the x-ray absorption fine structure (EXAFS) of K_2RbC_{60}, K_2CsC_{60}, Rb_2CsC_{60} and Rb_3C_{60} employing the K edges of potassium and rubidium as well as the L_{III} edge of cesium. The measurements were performed in transmission mode using Si(111) and Si(311) double crystal monochromators at the EXAFS-II and RÖMO-II beamlines of HASYLAB (DESY, Hamburg). Energy calibration was performed by measuring simultaneously reference compounds (KCl, RbCl, and CsCl). The higher harmonics were suppressed by detuning the monochromator to 40% of the maximum x-ray flux; the suppression was further enforced by the use of Ni or Au coated focusing mirrors at the EXAFS-II

TABLE I. Lattice parameters a_0 at room temperature and superconducting transition temperatures T_c. The data are from Refs. 17–20.

	Rb_2CsC_{60}	Rb_3C_{60}	K_2CsC_{60}	K_2RbC_{60}
a_0	14.460(1) Å	14.434(6) Å	14.292(1) Å	14.258(4) Å
T_c	32.5 K	29.5 K	24.0 K	21.5 K

beamline, used for the studies at the potassium K edge and the cesium L edges. The data reduction procedure followed the usual way as described in Ref. 14. Theoretical XAFS calculations (FEFF5.05) (Refs. 15 and 16) are used for the EXAFS analysis. The So^2 factors were set to 1.

The K_2CsC_{60} and Rb_2CsC_{60} samples were prepared in a two-step procedure, where at first doubly sublimed C_{60} and the respective alkali metals were reacted to phase-pure A_6C_{60} compounds. Appropriate amounts of these precursors were used together with C_{60} to prepare the A_2BC_{60} compounds. For K_2RbC_{60} and Rb_3C_{60} only purified C_{60} was used. The samples were characterized by x-ray diffractometry and ac-susceptibility measurements (see Table I for lattice parameters and T_c values).[17–20] The Rb_2CsC_{60} sample exhibit with $T_c = 32.5$ K the highest transition temperature of A_2BC_{60} systems and a remarkable sample quality as evidenced by the XRD diffractogram and the large diamagnetic shielding fraction.[18]

Homogeneous absorbers for the x-ray absorption studies were prepared by mixing appropriate amounts of finely ground sample material with (degassed) boron nitride. The mixtures were placed in vacuum-tight stainless-steel capsules and pressed between two Be windows to ensure an appropriate thermal contact and homogeneous absorber thickness. Sample handling was performed in a glovebox under purified argon atmosphere (with some residual helium). The samples were cooled in He-flow cryostats in the temperature range between 14 and 300 K. The sample temperature was measured with a calibrated Si diode and controlled within ± 1 K during the x-ray absorption measurements.

III. EXPERIMENTAL RESULTS AND DATA ANALYSIS

A. Raw data evaluation, $\chi(k)$ spectra and Fourier transforms

Figure 1 shows a representative selection of original x-ray absorption spectra (XAS) of K_2CsC_{60} and Rb_2CsC_{60} measured at temperatures of 20 K. They all exhibit a marked near-edge structure (XANES) and an extended fine structure (EXAFS), whose intensity decreases strongly with increasing temperature. The XANES structure can give already, as shown in Ref. 12, some structural information (fingerprints) about the site occupation. Here we concentrate on the EXAFS features. Figure 2 exhibits the EXAFS oscillations $\chi(k)$ obtained after data reduction of the XAS spectra.[14] It is evident for all three systems that the respective $\chi(k)$ spectra of the A and B ions exhibit drastic differences in the same A_2BC_{60} system indicating already a strong site preference. These differences are not due to the different alkali ions, since the spectra of the respective A and B ions in different A_2BC_{60} systems look quite similar, but are obviously different between A and B due to different site locations. This is strikingly demonstrated by the rubidium $\chi(k)$ spectra in Rb_2CsC_{60} and K_2RbC_{60}. This behavior is further corroborated by the Fourier transforms (FT) of the $\chi(k)$ spectra shown in Fig. 3 for the A ions and in Fig. 4 for the B ions except for Rb in K_2RbC_{60}. The more complex structures observed there will be discussed later. The A ion FT spectra (A=K, Rb) are very similar and exhibit two prominent peaks, which are attributed, as demonstrated in Sec. III B, to tetrahedral sites with carbon atoms in the nearest neighbor (NN) and next-nearest neighbor (NNN) shell, respectively. The principal structures remain unchanged with increasing temperature. The B ion FT spectra (B=Rb, Cs) exhibit less-resolved and broadened structures with concomitantly smaller amplitudes; both features are drastically reduced with increasing temperature and are attributed to the properties of the octahedral site. The most dramatic difference between A and B ion FT spectra is shown by the rubidium FT spectra of Rb_2CsC_{60} and K_2RbC_{60}, respectively. It should be mentioned that all Fourier transforms were performed in the same way, so the spectral features (including amplitudes) of the FT spectra in Figs. 3 and 4 are comparable for the three alkali ions.

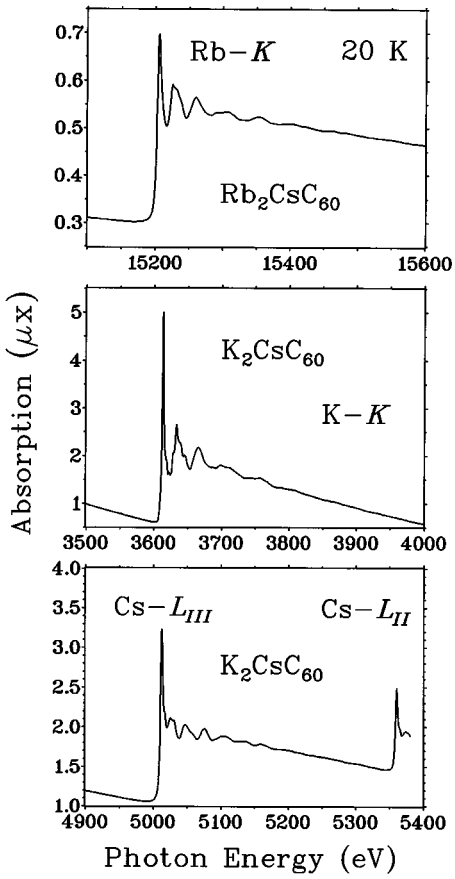

FIG. 1. Original x-ray absorption spectra at $T = 20$ K for Rb, K, and Cs in K_2CsC_{60} and Rb_2CsC_{60}. For rubidium and potassium the K edges and for cesium the L_{III} edges were measured.

From the above spectral features there is ample evidence that the smaller (larger) alkali metals occupy preferentially the tetrahedral (octahedral) sites. This is also expected from the stoichiometry of the samples and the fact that the lattice

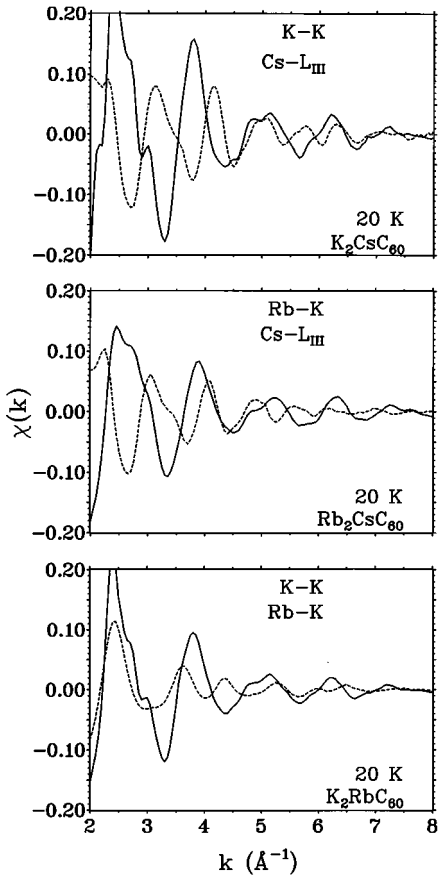

FIG. 2. EXAFS oscillations $\chi(k)$ at 20 K for K, Rb, and Cs in K_2CsC_{60}, K_2RbC_{60}, and Rb_2CsC_{60}. The continuous line describes K or Rb K edge spectra of tetrahedral sites, the dashed line describes Cs L_{III}-edge or the Rb K-edge spectra of the octahedral sites (the L_{III}-edge oscillations have a phase shift of 180° with respect to the K-edge spectra).

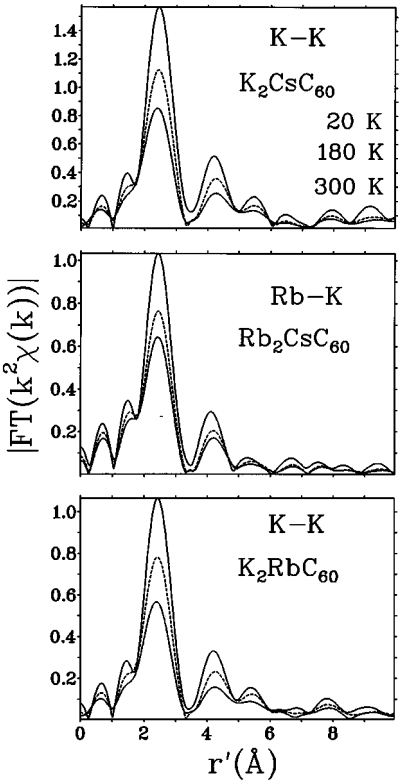

FIG. 3. Magnitude of the Fourier transforms of the tetrahedral site EXAFS in A_2BC_{60} at different temperatures. The transforms are k^2 weighted using the k range $1.8 \leq k/(\text{Å}^{-1}) \leq 6.0$. The Fourier forward transformation is performed after applying a square window.

parameters a_0 of our A_2BC_{60} samples exhibit only a small increase in comparison to the respective A_3C_{60} systems (see Table I). Preferential site occupation emerges also from Rietveld analyses of the XRD data performed for the present samples.[21] Striking evidence for site preference of the alkali ions is found furthermore in ^{87}Rb-NMR studies of the present Rb_3C_{60}, K_2RbC_{60}, and Rb_2CsC_{60} samples.[22]

B. EXAFS analysis of the tetrahedral sites in A_2BC_{60}

The A site FT spectra in Fig. 3 show two well separated peaks indicating well defined first and second neighbor shells. The first shell should originate, according to the structural features of the tetrahedral site, from the carbon neighbors arranged in four hexagons of the four neighboring C_{60} molecules. Before starting with a single-shell EXAFS analysis, a simulation of the EXAFS spectrum arising only from the first neighbor shell is appropriate. Figure 5 presents as example the Fourier-transformed simulations of Rb EXAFS in the tetrahedral sites of Rb_2CsC_{60} assuming carbon neighbors only in the first shell and, for comparison, in the first and second shell. The very good agreement for the first peak in the simulated and measured spectra (*position* and *amplitude*, the latter with a reasonable second cumulant) indicates, on the one hand, that our assumption made about a strong site preference is on a sound basis and allows us, on the other hand, to analyze the properties of the A ions at the tetrahedral site by a single-shell analysis. From the XRD data of Rb_2CsC_{60} one derives a distance of $R(A-C)=3.36(1)$ Å to the first carbon shell with an coordination number of $N_C=24$. The second shell consists of 24 next-nearest carbon neighbors at $R_2(A-C)=4.64(1)$ Å. This rather large difference in distance between first and second neighbor shell allows a separation of the first neighbor shell using the Fourier filtering technique. Figure 5 demonstrates also (upper part) that the second peak in the FT originates mainly from the second C shell. We will use this information for a multishell analysis of the tetrahedral site described below.

As an example for a single-shell analysis of an A ion in a tetrahedral site we show in Fig. 6 the backtransformed, filtered spectrum of Rb in Rb_2CsC_{60} at 20 K. The respective $\chi(k)$, FT and simulation spectra are shown in Figs. 2, 3, and 5. The EXAFS analysis needs in the harmonic approximation four parameters: the nearest neighbor distance, R_{A-C}, the mean-squared variation of R_{A-C}, σ^2 (also called second cumulant), the coordination number, N_C, and the zero energy of the free electron states, E_0, defining the starting point of the EXAFS oscillations. For a series of spectra measured as a function of temperature, the analyses were performed in the sequence.

(i) Identical raw data handling, energy calibration and background subtraction in an automated routine for all spectra of the series.

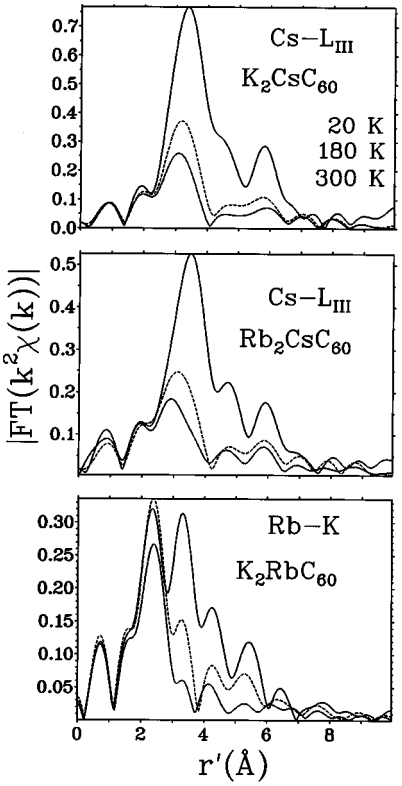

FIG. 4. Magnitude of the Fourier transforms of the octahedral site EXAFS in A_2BC_{60} at different temperatures. The transforms were performed identically to Fig. 3.

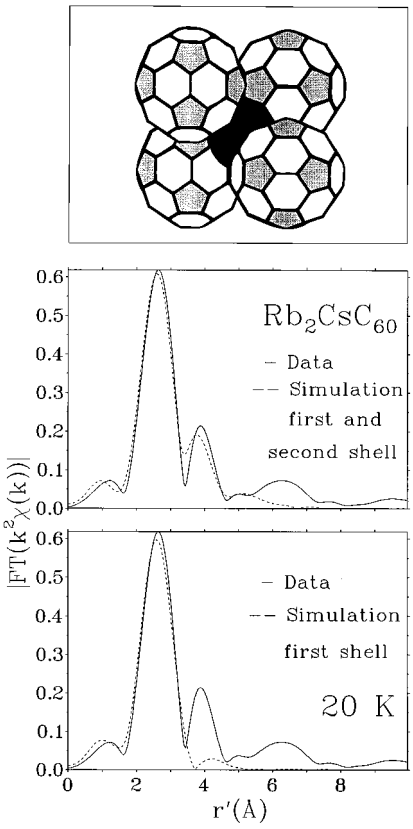

FIG. 5. (above) Schematic structure for the tetrahedral site. Magnitude of the Fourier transforms of the tetrahedral site EXAFS in Rb_2CsC_{60} at $T=20$ K and EXAFS simulations for the first neighbor shell (below) and for the first and second neighbor shell (middle). The Fourier forward transforms are k^2 weighted using a Hanning window in the k range $1.8 \leqslant k/(\text{Å}^{-1}) \leqslant 6.0$.

(ii) Single-shell analysis with free parameters (including E_0) with identical settings of the respective windows and transformation ranges (see Fig. 6),

(iii) Plot of the resulting values of R_{A-C}, N_C, and σ^2 as a function of temperature; the values of N_C and σ^2 are strongly correlated, especially at higher temperatures.

(iv) Extraction of averaged values for N_C and E_0; the value of N_C is not expected to vary, at least between 20 and 200 K.

(v) Repeated single-shell analysis, but now with fixed values of N_C and E_0. This procedure reduces strongly the numerical errors of the relevant parameters $R_{A-C}(T)$ and $\sigma^2(T)$.

The strong correlation between N_C and σ^2 is a well-known problem in the EXAFS analysis.[14] As just stated, we avoided this correlation in the analysis of the temperature-dependent series by fixing N_C to averaged values. The reliability of the averaged N_C values was checked then by fitting the data with different k spaces. Since σ^2 and N_C are depending differently on k, it is expected that the fits with a properly fixed value of N_C will show the same value of σ^2 when the k space is changed. The numerical error of the N_C values was determined by using fixed values of σ^2 within their error bars and looking for the variation of N_C. This procedure was performed with the low-temperature data.

The values of $R_{A-C}(T)$ and $\sigma^2(T)$ obtained from these fits for K in K_2RbC_{60} and K_2CsC_{60} as well as for Rb in Rb_2CsC_{60} are shown in Fig. 7 and Fig. 8, respectively. The derived nearest-neighbor distances are in excellent agreement with values of the A_t-C distances calculated from XRD data[1,3,4] in the respective systems at 300 K (see Table II). The observed temperature dependence of the $A-C$ distance, $R_{A-C}(T)$, can be used to extract the temperature dependence of the lattice constant. For this purpose we assume that the size of the C_{60} molecules does not change with temperature; the lattice constant $a_0(T)$ can be obtained from the following equation:

$$R_{A-C}(T)=\left| a_C\begin{pmatrix} C_x \\ C_y \\ C_z \end{pmatrix} - a_0(T)\begin{pmatrix} \frac{1}{4} \\ \frac{1}{4} \\ \frac{1}{4} \end{pmatrix} \right|, \qquad (1)$$

where $a_C(C_x,C_y,C_z)$ is the position of a C neighbor in a hexagon facing the A $(\frac{1}{4},\frac{1}{4},\frac{1}{4})$ site and belonging to a C_{60} molecule centered at the (0,0,0) position. From the linear slope of $R(T)$ in the temperature region 100 to 300 K, we derive thermal expansion coefficients $\alpha=\delta \ln a_0(T)/\delta T$ ranging from $2.1–3.3\times10^{-5}$ K^{-1} (see Table II). These values agree, within the error bars, with the ones given for C_{60}, K_3C_{60} and Rb_3C_{60} in Refs. 4 and 5.

The derived coordination numbers N_C of 23(2) and 24(2) for K_2CsC_{60} and Rb_2CsC_{60} indicate, within the accuracy (10%) of N_C, a full site ordering of the K and Rb ions in the tetrahedral sites. This finding implies also a high degree of orientational order of the C_{60} environment. The smaller value

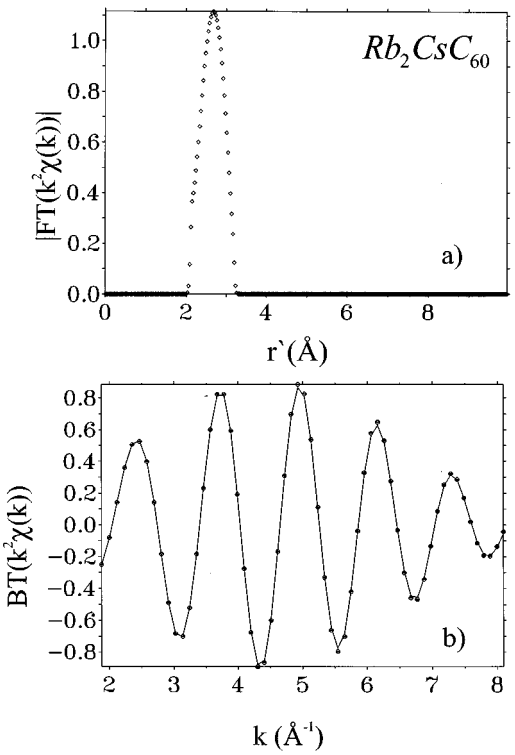

FIG. 6. Single-shell analysis of the tetrahedral site EXAFS in Rb_2CsC_{60}. (a) Filtered part of the Fourier transformed, k^2 weighted $\chi(k)$ spectrum using a Gauss window $[2.0 \leqslant r'/(\text{Å}) \leqslant 3.23]$. The Fourier forward transformation is performed after applying a square window $(1.9 \leqslant k/(\text{Å}^{-1}) \leqslant 8.1)$. (b) Backtransformed k^2 weighted $\chi(k)$ spectrum and single-shell analysis.

of $N_C = 18(2)$ for the K_2RbC_{60} sample can be explained by disorder effects (no perfect site preference of the potassium ions for the tetrahedral sites as well as rotationally disordered C_{60} positions), which is also reflected by the $\sigma^2(T)$ plots discussed next. The present K_2RbC_{60} sample was prepared from single-purified C_{60}, which resulted in a lower sample quality as evidenced already by a larger amorphous background in the XRD diffractogram[17,19] as well as by a smaller superconducting fraction and other magnetic shielding properties,[20] when compared with samples from doubly sublimed C_{60}.

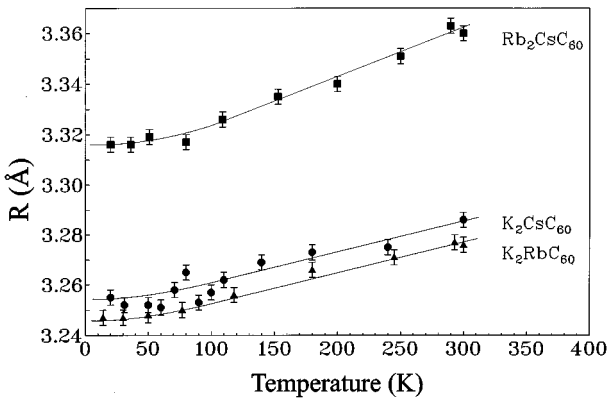

FIG. 7. Single-shell $A_t - C$ distances of the tetrahedral sites in A_2BC_{60} as a function of temperature.

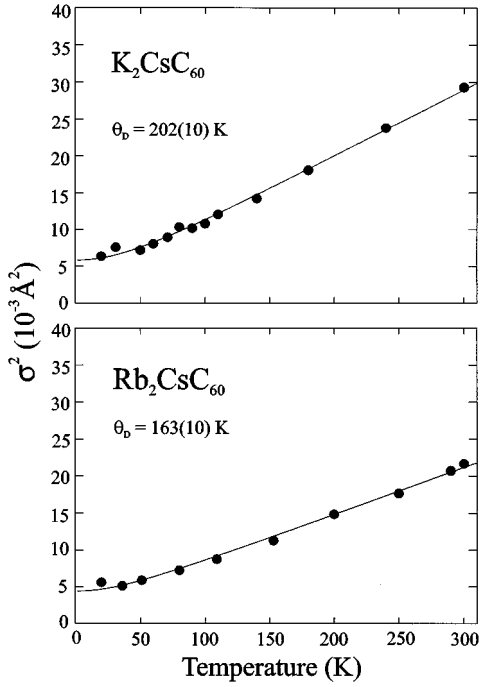

FIG. 8. Single-shell second cumulants, $\sigma^2(T)$, of the tetrahedral sites in A_2BC_{60} as a function of temperature. The solid line represents a Debye model fit, where the extracted local Debye temperatures $\Theta_D(A)$ are denoted.

The temperature variation of $\sigma^2(T)$ shown in Fig. 8 reveals important information on the local dynamic behavior and binding strength of the alkali ions in the tetrahedral sites. It can be used to derive local Einstein or Debye temperatures. Since the highly coordinated surrounding of the A site is resembling a solid more than a molecule, we fitted $\sigma^2(T)$ within the Debye formalism.[23] The derived EXAFS Debye temperatures, $\Theta_D(A)$, of the alkali metals A in the tetrahedral positions (see Fig. 8 and Table III) are comparable with those observed in alkali-halide systems. They are about equal for the same alkali ion with $\Theta_D(K) \approx 200$ K in the K_2RbC_{60} and K_2CsC_{60} systems and $\Theta_D(\text{Rb}) \approx 165$ K in Rb_2CsC_{60} and Rb_3C_{60} and scale, as expected for the same binding strength,

TABLE II. Coordination numbers N_C of the tetrahedral site ions (theoretical value $N_C = 24$), nearest-neighbor distances $R(A-C)$ at room temperature (from EXAFS analysis) and corresponding values calculated according to Eq. (1) from XRD results with a_0 values from Table I and C positions given in Ref. 4 assuming that the carbon positions on the C_{60} molecules remain unchanged. The given errors for $R(A-C)_{\text{XRD}}$ take into account the errors of a_0, a_C, and C_i $(i = x,y,z)$. The errors for $R(A-C)$ include numerical and systematic errors, the latter possible from the phase shift calculations. The relative errors for $R(A-C)$ values within a series as given in Fig. 7 are 0.003 Å. The errors for the Rb_3C_{60} system are larger due to the difference spectra.

	Rb_2CsC_{60}	Rb_3C_{60}	K_2CsC_{60}	K_2RbC_{60}
N_C	23(2)	21(3)	24(2)	18(2)
$R(A-C)$	3.360(10) Å	3.344(12) Å	3.286(10) Å	3.275(10) Å
$R(A-C)_{\text{XRD}}$	3.36(1) Å	3.33(2) Å	3.29(1) Å	3.28(1) Å
α $(10^{-5}\ \text{K}^{-1})$	3.3(2)	2.3(3)	2.1(2)	2.2(2)

TABLE III. EXAFS Debye temperatures $\Theta_D(A)$ of the tetrahedral site ions calculated from $\sigma^2(T)$ within the Debye model (Ref. 23) using the mass of A. (*) The value of Rb_3C_{60} is calculated from difference spectra. (**) The values for the A_6C_{60} systems are from Ref. 25. Values of bulk Debye temperatures Θ_D for the alkali-metal halides used as reference systems are obtained from heat-capacity measurements in the liquid helium region (Ref. 24).

	$\Theta_D(A)$	Reference	Θ_D (specific heat)
K_2RbC_{60}	193(10) K	KCl	235 K
K_2CsC_{60}	202(10) K	KBr	174 K
K_6C_{60}(**)	182(10) K		
Rb_2CsC_{60}	163(10) K	RbCl	165 K
Rb_3C_{60}(*)	167(10) K	RbBr	131 K
Rb_6C_{60}(**)	157(10) K		

roughly inversely with the square root of their mass. They are slightly larger than the ones derived for K and Rb from a similar EXAFS study of the K_6C_{60} and Rb_6C_{60} systems.[25] We take our results for $\Theta_D(A)$ as evidence that the A ions form an ionic bond with the surrounding C_{60}^{3-} molecules comparable to the alkali halides (but not as evidence that the tetrahedral cations are fully ionized).

The $\sigma^2(T)$ plots shown in Fig. 8 provide, as mentioned above, information about the sample quality. For a perfectly ordered nearest-neighbor environment with $N_C=24$, the extrapolation of $\sigma^2(T)$ to 0 K by a straight line should intersect the abscissa exactly at zero. This is almost the case for the K_2CsC_{60} and Rb_2CsC_{60} samples ($\Delta\sigma^2=1.3\times10^{-3}$ Å^2 and 1.8×10^{-3} Å^2); the K_2RbC_{60} sample, on the other hand, exhibits an offset ($\Delta\sigma^2=3.8\times10^{-3}$ Å^2) at $T=0$ K more than twice as large, pointing to an increased static disorder in agreement with the other findings discussed above, and originating intrinsically from the less pure C_{60} material used for the preparation.

Finally we want to present in this section a more complex analysis of the tetrahedral site properties. In Fig. 5 it was already demonstrated that the first two peaks in the A-site FT spectrum can be quite well reproduced by a two-shell EXAFS simulation. For the Rb sites in Rb_2CsC_{60} we performed a two-shell EXAFS analysis of the 24 nearest (NN) and 24 next nearest (NNN) carbon neighbors including five multiple scattering paths. The properties of the second shell were constrained by constant ratios known from the structural parameters. Figure 9 shows the results of this two-shell analysis. The good agreement of the backtransformed $\chi(k)$ spectrum demonstrates that also the second neighbor shell is well described by this approach. This implies, on the one hand, that the FEFF5 code used[15,16] is well suited to calculate the theoretical phase shifts and amplitudes as well as the contributions from the multiple scattering paths even for low-Z neighbors such as carbon. The agreement is, on the other hand, a further proof of the orientational order of the C_{60} molecules within the space group $Fm3m$. Any rotational disorder of the C_{60} molecules, i.e., hexagons not oriented along the (111) axis, should have a larger impact on the second-neighbor shell as well as on the multiple-scattering amplitudes resulting in a stronger fading of the spectral features than for the first shell.

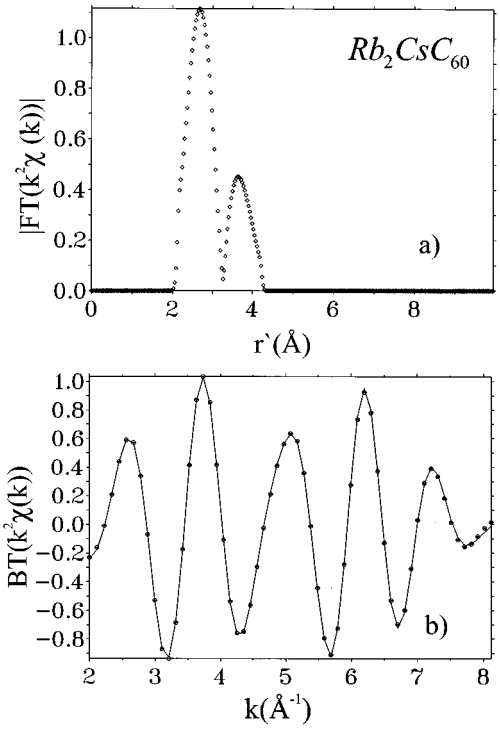

FIG. 9. Multishell analysis of the tetrahedral site EXAFS in Rb_2CsC_{60}. (a) Filtered part of the Fourier transformed, k^2 weighted $\chi(k)$ spectrum using a Gauss window ($2.0\leqslant r'/(\text{Å})\leqslant4.27$). The Fourier forward transformation is performed after applying a square window ($2.0\leqslant k/(\text{Å}^{-1})\leqslant8.1$). (b) Backtransformed k^2 weighted $\chi(k)$ spectrum and multishell analysis assuming seven different scattering paths.

C. EXAFS analysis of tetrahedral sites in Rb_3C_{60}

The analysis of A_3C_{60} spectra is more difficult because both tetrahedral and octahedral sites are occupied by the same atomic species. One could of course try to adjust the tetrahedral and octahedral sites simultaneously. But since the analysis of the octahedral sites is rather complex (see next the section) and their contributions to the $\chi(k)$ spectra are small, we used a different approach by calculating difference spectra from A_3C_{60} and the respective A_2BC_{60} systems, here Rb_3C_{60} and K_2RbC_{60}. Such a procedure is possible since the structural properties of the respective A and B sites are very similar in different A_2BC_{60} and A_3C_{60} systems as reflected by the lattice constants (see Table I). Difference spectra (such as the summation of spectra) require a good energy calibration for each spectrum; we used the same reference compound during the measurements. After energy calibration the spectra were normalized. For subtraction one has to consider the ratio 2:1 between tetrahedral and octahedral sites. Therefore the normalized Rb_3C_{60} spectra consist of contributions arising to $\frac{2}{3}$ from the tetrahedral sites and to $\frac{1}{3}$ from the octahedral sites. For calculation of the difference spectra reflecting solely the properties of the tetrahedral sites, we subtracted the $\frac{1}{3}$ weighted Rb spectra of K_2RbC_{60} from the Rb_3C_{60} spectra and renormalized the difference spectra. A typical $\chi(k)$ spectrum and its Fourier transform of the tetrahedral sites in Rb_3C_{60} is shown in Fig. 10 together with the equivalent Rb_2CsC_{60} system. A set of difference spectra of data from a temperature scan of Rb_3C_{60} was used for

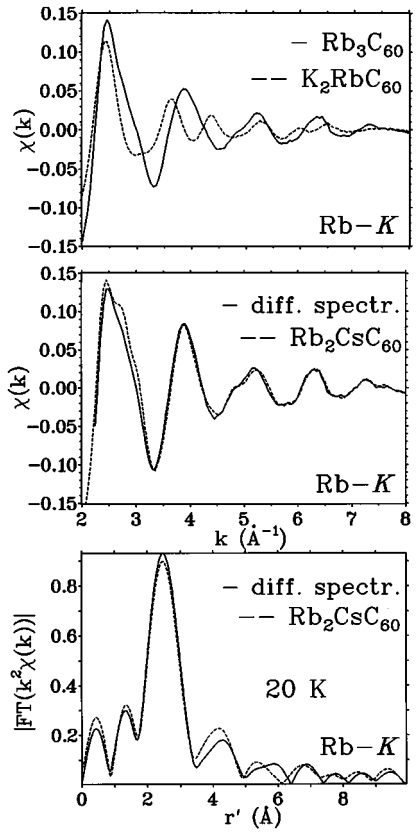

FIG. 10. (above) EXAFS oscillations $\chi(k)$ at $T=20$ K for Rb in Rb_3C_{60} and K_2RbC_{60}. (middle) Difference spectrum of the above spectra, $3/2(Rb_3C_{60}-1/3K_2RbC_{60})$, and spectrum of Rb_2CsC_{60} at 20 K. (below) Magnitude of the Fourier transforms of $3/2(Rb_3C_{60}-1/3K_2RbC_{60})$ and Rb_2CsC_{60}. The transforms are k^2 weighted using a k range $2.3\leqslant k/(\text{Å}^{-1})\leqslant 6.0$. The Fourier forward-transformation is performed after applying a square window.

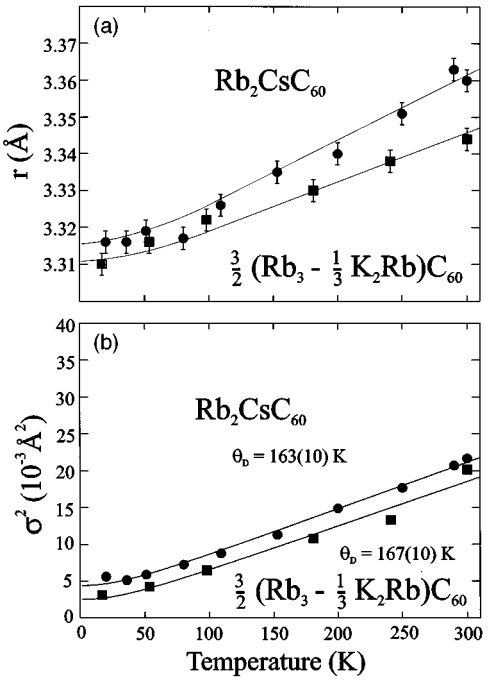

FIG. 11. Single-shell analysis of the tetrahedral site EXAFS spectra of $3/2(Rb_3C_{60}-1/3K_2RbC_{60})$ and Rb_2CsC_{60}: (a) A_t-C distances of the tetrahedral sites, (b) second cumulants (σ^2) of the tetrahedral sites. The solid line represents a Debye model fit where the local Debye temperatures Θ_D(Rb) are extracted.

single-shell EXAFS analysis of the tetrahedral site. The resulting temperature dependence of $R(A-C)$ and $\sigma^2(T)$ is shown in Fig. 11 and derived values are compiled in Tables II and III. The very good agreement of the tetrahedral site spectra of Rb_3C_{60} and Rb_2CsC_{60} shown in Fig. 10 as well as the derived structural properties support our approach for the calculation of difference spectra. It should be mentioned that difference spectra were also successfully used to extract information about the tetrahedral and octahedral site properties from the corresponding XANES spectra.[12,28] A possible occupation of the tetrahedral A sites by 10% of the Rb ions, which was found as the upper limit in the ^{87}Rb-NMR study of the present K_2RbC_{60} sample, would influence slightly the derived values of N_C and $\sigma^2(T)$ within the given error bars, but not the $R_1(A-C)$ values.

D. EXAFS analysis of the octahedral sites in A_2BC_{60}

The B ion spectra displayed in Figs. 2 and 4 and comparison with the corresponding features of the A ion spectra in Figs. 2 and 3 reveal basic differences in the local site properties of A and B ions. Assuming a centered position in the octahedral site, the B ions should have 12 nearest carbon neighbors at a distance $R_{1c}(B-C)=3.70-3.80$ Å, depending on the lattice parameter, and 24 next-nearest carbons at a distance $R_{2c}(B-C)=4.5-4.6$ Å. This situation is different from the tetrahedral site due to the larger distance and the smaller coordination number of the first carbon shell. One should also consider the fact that the separation between first and second shell decreases from 1.3 Å for the tetrahedral site to 0.8 Å for the octahedral site. This renders a single-shell analysis of the octahedral site, even for a centered position, less appropriate. Indeed, all our attempts to simulate or fit the B ion spectra by a single-shell were not successful, especially for the spectra measured at low temperatures, where the spectral features indicate a more complex surrounding.

There is, however, a more important reason for the failure of a *single-shell* analysis for the octahedral sites as demonstrated in Fig. 12 by *multishell simulations* of the $\chi(k)$ spectra and the corresponding FT spectra of Cs in K_2CsC_{60}. These simulations assume a *centered* position of Cs on the octahedral site and includes contributions from eight carbon neighbor shells and the tetrahedral K ions up to 8.2 Å as well as from all multiple scattering paths with 3 or 4 legs. Obviously, the simulated $\chi(k)$ and FT spectra do not agree with the measured $\chi(k)$ and FT spectra. Especially the measured $\chi(k)$ spectrum shown in Fig. 12 is different in exhibiting an opposite phase in comparison to the simulated spectrum. The corresponding FT spectra are shifted in their maxima (by about 0.3 Å at 300 K) to smaller distances in comparison to the simulated FT spectra. The real and imaginary parts of the FT spectra (not shown) also demonstrate, as evidenced already by the $\chi(k)$ spectrum, that the measured and simulated spectra are built up from neighbor shells different in radii and coordination numbers. These features provide direct evidence for an off-center position of the Cs ions at the octahedral sites in K_2CsC_{60}.

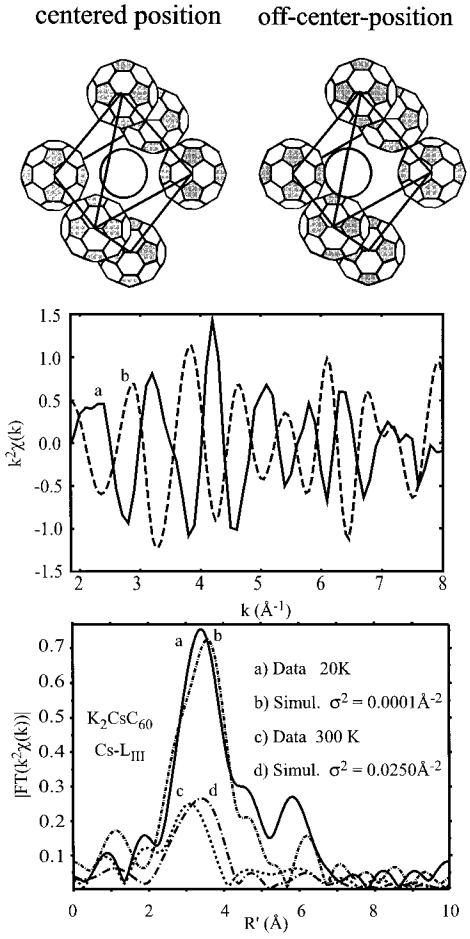

FIG. 12. (above) Schematic presentation of the octahedral site with a centered (left) and an off-center (right) position of the B ion. (middle) Experimental Cs-L_{III} $\chi(k)$ spectrum of K_2CsC_{60} as measured at 20 K (solid line) and corresponding simulated $\chi(k)$ spectrum assuming a centered position (dashed line). (below) Fourier forward transforms of experimental (a) and (c) and simulated (b) and (d) $\chi(k)$ spectra at 20 K and 300 K, respectively. The FT spectra are k^2 weighted using a Hanning window in the k range $1.8 \leqslant k/(\text{Å}^{-1}) \leqslant 6.0$.

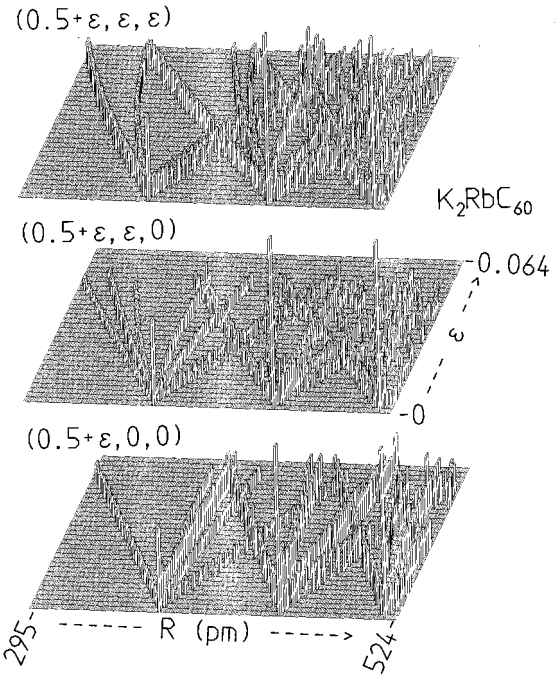

FIG. 13. Histograms of the carbon neighbor distance distribution, $R_i(B-C)$, for an off-center displacement in the $(0.5+\epsilon,0,0)$, $(0.5+\epsilon,\epsilon,0)$ and $(0.5+\epsilon,\epsilon,\epsilon)$ direction of K_2RbC_{60} (ϵ is the fraction of the unit cell). On the abscissa the first, second, and third carbon neighbor shell with coordination numbers 12, 24, and 24 (as reflected by the height of the bars) is given for a centered position ($\epsilon=0$). The displacements are calculated until the R_1(Rb-C) distance reach values limited by the ionic radii. The same presentation can be used for the Cs ions on octahedral sites in K_2CsC_{60} and Rb_2CsC_{60} considering the different $R_{ic}(B-C)$ values.

Similar simulations and comparison with the experimental $\chi(k)$ and FT spectra indicate that also the Cs ions on the octahedral sites in Rb_2CsC_{60} exhibit distances to the neighboring carbons which are by about 0.4 Å shorter than expected for a centered position. In the case of K_2RbC_{60}, the FT spectra shown in Fig. 4 point to an even larger off-center position of the Rb ions on the octahedral sites. The marked peak at $r'=2.3$ Å in the Rb-EXAFS-FT spectra originates, as proved by the $\chi(k)$ spectra and simulations, from a complex multishell surrounding with a variety of distances. Possible contributions from B ions on tetrahedral sites to this peak will be discussed later.

Simple geometrical considerations reveal that nearest $B-C$ distances shorter by about 0.3 to 0.6 Å than expected for a centered position result in off-center displacements Δ being of about the same magnitude, when the displacement points in the (1,0,0) direction, or being roughly $\sqrt{2}$ and $\sqrt{3}$ times larger for displacements in the (1,1,0) and (1,1,1) directions, respectively. Such off-center positions of the B ions on the octahedral sites demand for a new strategy for the analysis of the EXAFS spectra in terms of neighbor shells. With increasing off-center displacement Δ the original neighbor shells with defined distances and high coordination numbers split into a variety of subshells with lower coordination numbers. We demonstrate this behavior in Fig. 13, where the influence of displacements of B ions in the (1,0,0), (1,1,0) and (1,1,1) directions on the neighbor shells is shown.

If one assumes that the B ions are randomly displaced in all crystallographic directions, one would end up with a broad distribution of $R_i(B-C)$ distances, which could not be adjusted by a multishell analysis, but only described by a distribution function. Obviously, the $\chi(k)$ and FT spectra of the octahedral sites exhibit some structures, being more defined at low temperature (see Figs. 2, 4, and 12). This excludes a random distribution and points to a position of the B ions determined mainly by a close contact with (as many as possible) neighboring carbons, and hence by the radii of the alkali ions and the structural properties of the octahedral sites. The most favorable position is now known *a priori*, but the present B-site EXAFS analysis together with the information contained in Fig. 13 as well as chemical and structural arguments may give some information about the most probable off-center displacement direction.

In the B-site EXAFS analysis we used a multishell approach allowing four carbon neighbor shells to account for the large variety of possible neighbor configurations. The window settings in the respective r' spaces were chosen con-

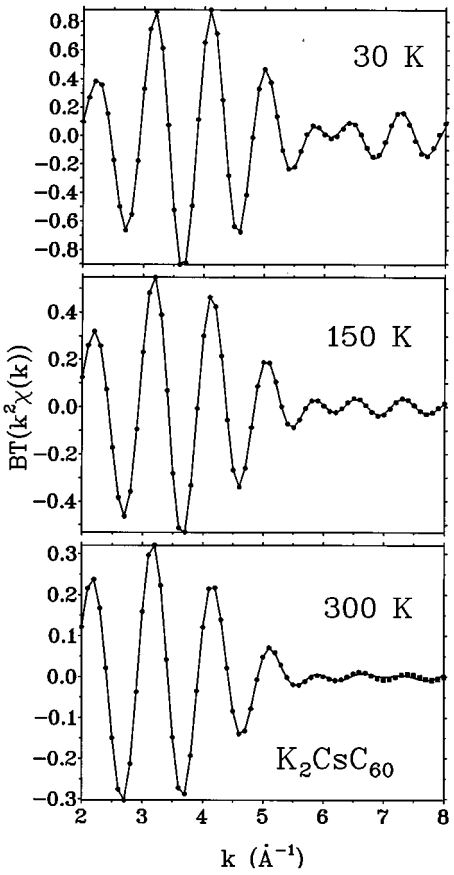

FIG. 14. Four-shell fit of the back-transformed octahedral site Cs-L_{III} $\chi(k)$ spectra in K_2CsC_{60} at different temperatures [the transformation ranges are $1.8 \leqslant k/(\text{Å}^{-1}) \leqslant 8.1$ and $1.5 \leqslant r'/(\text{Å}) \leqslant 4.9$].

siderably larger than in the case of the two-shell analysis of the tetrahedral Rb site (compare captions of Fig. 9 and Fig. 14). A large variety of starting parameter sets was tried for the four-shell fits in the first steps of the analysis; finally similar solutions emerged describing quite well the properties of all B sites spectra at low temperature. These parameter sets were then used in the fitting procedure of the temperature series. A final refinement was obtained, similar to the procedure described above for the analysis of the tetrahedral A ions, by fixing the respective N_i values and E_0 within a series to averaged values obtained from low-temperature (20–100 K) spectra. The second cumulants σ_i^2 of the $R_i(B-C)$ distances are significantly larger (by roughly a factor 2) than the ones derived for the tetrahedral sites and point, from their behavior at low temperature, to a distribution of distances within the shells as a consequence of the off-center position. Accordingly, the derived averaged values of N_i are highly correlated with σ_i^2 and have large error bars. The fourth shell, according to the fits located around 4.5–4.8 Å, contributes only to the low-temperature spectra and contains the further distant carbon shells and multiple scattering paths. Geometrical considerations and simulations show that the contributions of multiple scattering paths are decreasing for increasing off-center position of the B ions.

Typical results for the Cs L_{III}-EXAFS of K_2CsC_{60} and Rb_2CsC_{60} are presented in Figs. 14 and 15 showing the back-transformed $\chi(k)$ spectra and the temperature dependence of the $R_i(B-C)$ distances, respectively. The relevant fit results for the three B site systems are compiled in Table IV. From the Rb spectra of K_2RbC_{60} one derives a nearest octahedral Rb_0-C distance of 2.98 Å, definitely shorter than $Rb_t-C=3.33$ Å and 3.36 Å found for the tetrahedral sites in Rb_3C_{60} and Rb_2CsC_{60}. This nearest Rb_0-C distance is slightly larger than the distance expected from the ionic radius of Rb (1.47 Å) and the electronic radius of the C_{60} molecule (1.45 Å). As evidenced already by the spectral features in Figs. 2 and 4, the derived local structural properties of Cs in K_2CsC_{60} and Rb_2CsC_{60} are similar, but reflect also the different size of the octahedral site [as given by $R_{1c}(B-C)$ in Table IV]. The nearest Cs-C distances are somewhat larger (by ≈0.2 Å) than expected from the ionic radius (1.67 Å for Cs).

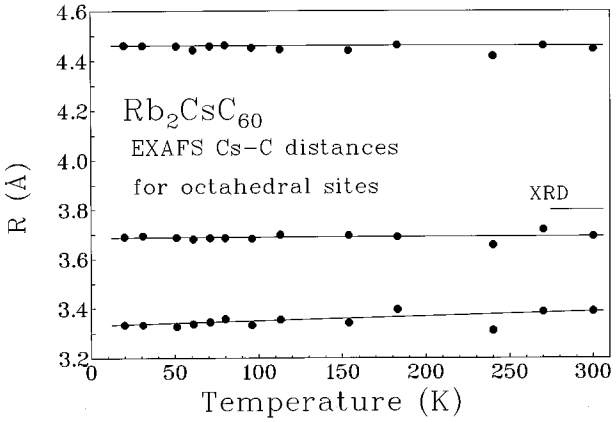

FIG. 15. $R_i(B-C)$ distances ($i=1$, 2, and 3) of the octahedral sites in Rb_2CsC_{60} as a function of temperature. The marker XRD gives the first neighbor distance in a centered position, $R_{1c}(B-C)$.

The structural features of the octahedral sites will be discussed now in more detail for the B ions in K_2CsC_{60}, Rb_2CsC_{60}, and K_2RbC_{60} with respect to the derived distances and coordination numbers of the three carbon shells. An off-center position on the octahedral site allows only a few nearest neighbors with short nearest $B-C$ distances, a situation completely different to the regular positions on tetrahedral sites. The histograms of neighbor distributions shown in Fig. 13 reveal only two nearest carbon neighbors

TABLE IV. Structural properties of B ions in octahedral sites: Coordination numbers N_i, neighbor distances $R_i(B-C)$ at room temperature and the value calculated for a central B-position $R_{1c}(B-C)$ with $N_{1c}=12$ and $N_{2c}=24$.

	Rb_2CsC_{60}	K_2CsC_{60}	K_2RbC_{60}
N_1	4(1)	4(1)	4(1)
$R_1(B-C)$	3.39(2) Å	3.27(2) Å	2.98(2) Å
N_2	10(2)	10(2)	12(2)
$R_2(B-C)$	3.69(3) Å	3.62(3) Å	3.32(3) Å
N_3	19(4)	19(4)	24(6)
$R_3(B-C)$	4.45(5) Å	4.40(5) Å	3.70(5) Å
$R_{1c}(B-C)$	3.80(1) Å	3.72(1) Å	3.70(1) Å
$R_{2c}(B-C)$	4.60(1) Å	4.51(1) Å	4.48(1) Å

for a displacement in the (1,0,0) direction and three neighbors for the (1,1,1) direction. A displacement in the (1,1,0) direction allow either 4, or 2+2, or 1+2+1 nearest carbons with slightly different distances, when the two neighboring C_{60} molecules are oriented parallel, in line or perpendicular with their edges, respectively (see Fig. 13). This behavior reflects the merohedral disorder of the C_{60} molecules. The observed values of N_1 are compatible with displacements in the (1,1,0) and (1,1,1) directions or in the various positions between these two directions. A defined (1,0,0) displacement seems less probable, this is also unlikely from stability arguments.

Considering the properties of possible next-nearest carbon shells in the three cases shown in Fig. 13, one realizes that next-nearest shells exhibit slightly larger (averaged) $R_2(B-C)$ distances than $R_{1c}(B-C)$ for displacements in the (1,0,0) and (1,1,0) directions. A (1,1,1) displacement, however, leads to next-nearest carbon shells with smaller $R_2(B-C)$ distances than $R_{1c}(B-C)$. The averaged second shell distances $R_2(B-C)$, listed in Table II, are smaller than the corresponding R_{1c} distances. This can be taken as evidence for a dominant displacement of the B ions in the (1,1,1) direction. Such a behavior can be explained by the argument that the B ions tend to have as many close contacts as possible with the neighboring carbons. A displacement in the (1,1,1) direction or in positions near to the (1,1,1) direction allows for the most additional close contacts with three neighboring C_{60} molecules and provides a relatively stable position, at least at low temperature. At elevated temperatures, additional positions may also become possible for the octahedral site.

From the observed $R_1(B-C)$ and $R_2(B-C)$ distances of the Cs ions in K_2CsC_{60} and Rb_2CsC_{60} one can estimate, according to Fig. 13, displacements with $\epsilon=0.030(2)$ in the (1,1,1) and also in the (1,1,0) direction. Many slightly different carbon neighbor surroundings are possible between these directions with no preferred position as discussed now for octahedral Rb.

The smaller cation size of Rb allows for larger displacements in the octahedral sites, as shown for K_2RbC_{60} in Fig. 13. Assuming a displacement in the (1,1,1) direction, one derives $\epsilon=0.058$ from the observed $R_1(B-C)$ and $R_2(B-C)$ distances. This is a special position, where a well-defined second shell with $N_2=6$ exists, which is built up from carbons belonging initially to the first and second shell. This may be, at low temperature, a stable position for octahedral Rb ions in K_2RbC_{60} and Rb_3C_{60}.

One should now comment on the fact that a small fraction of the B ions may occupy tetrahedral sites with $B-C$ distances close to $A-C$ distances, e.g., 3.3–3.4 Å. If one considers a 10% occupation of the tetrahedral site in K_2RbC_{60} by Rb as derived as *upper limit* from ^{87}Rb-NMR,[22] one obtains for the *tetrahedral* Rb ions an additional effective coordination number of $N_t\approx 5$ considering the coordination number 24 and the smaller second cumulant at the tetrahedral site; this may explain the observed coordination number of the second shell, $N_2=12(2)$, larger than expected for the above simulated (1,1,1) displacement. Similar considerations show that a 5% occupation of the tetrahedral sites in the present K_2CsC_{60} and Rb_2CsC_{60} samples, obtained as upper limits from Rietveld analysis and ^{87}Rb-NMR,[22] may increase the coordination number of the first shell by ≈ 1. This is within the error bars of these values, $N_1=4(1)$, and may also explain the higher values than expected for a (1,1,1) displacement. It should be mentioned here that an occupation of tetrahedral sites in K_2CsC_{60} by Cs should introduce large local disorder with reduced effective carbon coordination numbers. Therefore possible small fractions of Cs or Rb ions on tetrahedral sites may alter the coordination numbers of the first or second shell in the present analysis, but do not alter the basic findings about the properties of B ions on octahedral sites.

IV. DISCUSSION

A. Site preference and tetrahedral-site properties

The presented raw data, $\chi(k)$ spectra, and Fourier transforms demonstrate that the spectral features are dominated by the well-defined local structural properties of the tetrahedral sites. Detailed analyses of three A_2BC_{60} systems, K_2RbC_{60}, K_2CsC_{60}, and Rb_2CsC_{60}, reveal a strong site preference, where the smaller A ions occupy the tetrahedral sites and the larger B ions occupy the octahedral sites. These findings are in good agreement with previous studies of $A_{3-x}B_xC_{60}$ systems[7–11] and are further corroborated by x-ray diffraction studies[21] and ^{87}Rb-NMR measurements[22] performed on the same samples as used in our x-ray absorption experiments. In the case of K_2CsC_{60}, the Rietveld analysis revealed a site preference of at least 95%.[21] The ^{87}Rb-NMR measurements on Rb_2CsC_{60} and K_2RbC_{60} show a site preference of the Rb ions for the tetrahedral and octahedral sites by at least 95% and 90%, respectively.[22] These observations agree well with the observed coordination numbers for the tetrahedral sites in the EXAFS analyses.

The local structural and dynamic properties of the tetrahedral site cations in A_2BC_{60} and A_3C_{60} systems were determined with high precision by single-shell and double-shell EXAFS analysis in the temperature range 20–300 K. On the one hand, the results are supporting the structural knowledge based on XRD studies performed mostly at room temperature,[1,2,3,5] but give also further information about the low-temperature behavior. As an important result, the determination emerges of local Debye temperatures of the A ions from the second cumulants, indicating an ionic character of the bonding at the A ions with the surrounding C_{60} hexagons. The derived thermal expansion coefficients agree well with the few data available up to now on these systems. The second cumulants also provide, together with the coordination numbers, information about the sample quality and compares well with the information obtained from XRD spectroscopy and superconducting properties. The strong site selectivity in the A_2BC_{60} systems allowed an analysis of the tetrahedral sites in Rb_3C_{60} by creating difference spectra, eliminating the contributions of the octahedral sites by subtracting appropriately weighted Rb spectra of K_2RbC_{60}.

B. Octahedral sites: Local properties and off-center positions

The EXAFS results for the octahedral sites exhibit drastic differences in comparison to the analysis of the tetrahedral A sites. A reliable analysis was only possible with a multishell analysis revealing an off-center position with nearest neigh-

bor distances even shorter than observed for the tetrahedral sites. From the derived structural information contained in the first three carbon shells we developed for Rb in K_2RbC_{60} evidence for displacements in the (1,1,1) direction by simulating neighbor shells for displacements in various crystallographic directions. An off-center position $(0.5+\epsilon,\epsilon,\epsilon)$ with $\epsilon=0.058$ seems preferable for the Rb ion, since it allows for a well-defined new first and second neighbor shell, which might be stable at low temperature. One should note in this context a Rb-EXAFS study of closely related graphite intercalation compounds; namely, stage-1 RbC_8 with a regular Rb position between the carbon hexagons and stage-2 RbC_{24} with an off-center Rb position yielding also shorter Rb-*C* distances than for a regular position.[26]

For Cs in K_2CsC_{60} and Rb_2CsC_{60}, the off-center displacement is less pronounced reflecting the larger ionic radius of Cs. There is also evidence for a preferred displacement in the (1,1,1) direction, but displacements in the (1,1,0) direction or in between these two directions seem also possible.

The present EXAFS analysis about an off-center position for the octahedral site cations agrees with our preliminary report on K_2RbC_{60};[12] the present multishell analysis together with the use of the advanced FEFF5.05 phase-shift calculations,[15,16] however, improved the information about neighbor distances and coordination. During completion of this work we became aware of an Rb EXAFS study[27] of K_2RbC_{60} and Na_2RbC_{60} together with Rb_2CsC_{60} as reference system for the tetrahedral site. The authors also found evidence for off-center positions of Rb on the octahedral sites in K_2RbC_{60} and Na_2RbC_{60}.[27] From a single-shell analysis of a room-temperature EXAFS spectrum, they deduced a nearest Rb_0-C distance of 3.30(2) Å with a coordination of $N_C=3.4(2.1)$ in K_2RbC_{60}. This is not in conflict with the present results, since a single-shell analysis is averaging over the information obtained in our study mostly at low temperature. One should note that Hirosawa *et al.*[27] found in addition to their EXAFS results also evidence for a displacement in the $(0.5+\epsilon,\epsilon,\epsilon)$ direction from Madelung energy calculations (assuming C_{60} spheres). The calculated energy minima are well compatible with the off-center displacement derived in the present study.

Finally we want to mention that an off-center position directly emerges also from the near-edge structure (XANES) of the respective octahedral site ions, observed either directly in Cs L_I-edge spectra of K_2CsC_{60} and Rb_2CsC_{60} (Ref. 25) as well as in the Rb *K*-edge spectrum of K_2RbC_{60} or observed in difference spectra of the octahedral sites in K_3C_{60} (prepared by subtraction of the appropriately weighted K_2RbC_{60} spectrum) and in Rb_3C_{60} (prepared similarly with the Rb_2CsC_{60} spectrum).[12,28] The lower local symmetry of an off-center position leads to a splitting of the unoccupied *p* states of the *B* site ions, which is directly reflected in the respective Rb-*K* and Cs-L_I XANES spectra.[12,25,28]

We discuss now the information delivered by other methods with respect to an off-center position of the octahedral site ions. All XRD Rietveld analyses of A_3C_{60} and A_2BC_{60} diffractograms reveal an unusual large thermal parameter, $B=8\pi^2\langle u^2\rangle$, for the octahedral sites, being about four times larger than that for the tetrahedral site *A*, even at low temperatures. This *B* factor may reflect, as the second cumulant σ^2 in the present EXAFS analysis, beside the temperature effects also static disorder. In some of the XRD studies a possible off-center position is discussed. Reference 5 cites explicitly Rietveld analyses of Rb_3C_{60} data taken at room temperature and low temperature with the octahedral ions statistically dislocated in defined off-center positions such as $(0.5+\epsilon,0,0)$, $(0.5+\epsilon,\epsilon,0)$, or $(0.5+\epsilon,\epsilon,\epsilon)$, from which it was concluded that there is no compelling evidence for anything other than a spherically symmetric distribution of atomic density in the octahedral sites.[5] Rietveld simulations performed for the present A_3C_{60} systems[21] indicate that changes in the XRD pattern due to octahedral off-center positions are small and difficult to detect in comparison to other effects (e.g., rotational disorder of C_{60} molecules). In our opinion there is at present neither a proof nor a disproof of an octahedral off-center position from XRD analyses.

We now turn to NMR investigations of A_3C_{60} and related systems. As outlined in a recent ^{13}C-NMR study of some of the present samples,[29] the broad spectral features of A_3C_{60} systems, when compared with A_4C_{60} and A_6C_{60} systems, can be immediately explained by off-center positions of the octahedral alkali ions, introducing a variety of different carbon surroundings on the neighboring C_{60} molecules, either by direct $B-C$ interactions such as covalent admixtures of alkali *sp* orbitals or by indirect effects such as a charge redistribution on the C_{60} molecules due to nearer or more distant octahedral cations.

The ^{87}Rb-NMR spectra of Rb_3C_{60} exhibit three lines, two of them are attributed to the tetrahedral sites (T and T'), the other one to the octahedral site (O). The reason for the appearance of two different tetrahedral sites is still in discussion;[5,11,22,30] it is worth mentioning that Walstedt *et al.*[11] proposed an off-center displacement of the *O*-site cations in the (1,1,1) direction, creating T' sites with a nearer *O*-site cation surrounding and *T* sites with further distant *O*-site cation surrounding. This model is compatible with the present EXAFS results, the different *T* and T' sites observed in ^{87}Rb-NMR must originate from electronic differences, since structural differences can be excluded for the tetrahedral sites from XRD data and the present EXAFS investigations. It is of interest in this context that the ^{87}Rb-NMR spectrum of the present Rb_2CsC_{60} sample[22] exhibits also the T and T' line.

One should finally mention ^{13}C- and ^{87}Rb-NMR studies on Rb_3C_{60} (Ref. 30) performed over a wide temperature range, where strong hysteretic line broadenings and shifts of the ^{87}Rb lines were observed around 60 K and attributed speculatively to a structural phase transition. Since we found no evidence for a structural rearrangement between the tetrahedral site cations and the C_{60} molecules in this temperature region, one should consider a structural rearrangement of the octahedral Rb sites. As already discussed for K_2RbC_{60}, the (1,1,1) displacement offers a position with a rather defined first and second carbon neighbor shells, this position should be occupied at low temperature. The hysteretic line broadenings observed in the ^{87}Rb-NMR spectra around 60 K could be attributed to a freezing of the octahedral Rb in this position, while diffusive motions within the octahedral site may result in line-narrowing processes at higher temperatures.

Future K and Rb EXAFS and XANES studies should be devoted to unravel the properties of the octahedral sites in

systems such as K_3C_{60} and Rb_3C_{60}, especially at low temperatures. Systems such as Na_2RbC_{60}, showing no merohedral disorder would be also of interest as well as the high-temperature phases such as Rb_1C_{60}, where only the octahedral site is occupied.

ACKNOWLEDGMENTS

The authors would like to acknowledge the help of J. Dumschat during parts of the XAS measurements and for preparing the difference spectra; we thank M. Baenitz and M. Kanowski for supplying us with susceptibility and NMR data prior to publication and W. Bensch for his contributions to the Rietveld analyses. We want to thank J. J. Rehr for helpful discussions during the first steps of using the FEFF5 program, P. W. Stephens for his comments on Rietveld analyses and Ch. Hermes for useful discussions. This work was supported by the BMFT (Project No 05 5PPACB and the Pilotprojekt Fullerene) and by the DFG (Project No. Wo209/10).

[1] P. W. Stephens *et al.,* Nature **351**, 632 (1991).
[2] R. M. Fleming *et al.,* Nature **352**, 787 (1991).
[3] K. Tanigaki *et al.,* Nature **356**, 419 (1992); K. Tanigaki *et al.,* J. Phys. Chem. Solids, **12**, 1645 (1993).
[4] O. Zhou and D. E. Cox, J. Phys. Chem. Solids **53**, 1373 (1992).
[5] J. E. Fischer *et al.,* J. Phys. Chem. Solids **56**, 1445 (1995).
[6] P. W. Stephens *et al.,* Phys. Rev. B **45**, 543 (1992).
[7] Y. Maniwa *et al.,* J. Phys. Soc. Jpn. **62**, 3822 (1993).
[8] I. Hirosawa *et al.,* Solid State Commun. **82**, 979 (1992).
[9] I. Hirosawa *et al.,* Solid State Commun. **89**, 55 (1994).
[10] Y. Maniwa *et al.,* Solid State Commun. **82**, 1261 (1992).
[11] R. E. Walstedt, D. W. Murphy, and M. Rosseinsky, Nature **362**, 611 (1993).
[12] G. Nowitzke *et al.,* Mol. Cryst. Liquid Cryst. **245**, 321 (1994).
[13] G. Nowitzke *et al.,* Physica B **208&209**, 273 (1995).
[14] Boon K. Teo, *EXAFS: Basic Principles and Data Analysis* (Springer-Verlag, Berlin, 1986) ISBN 3-540-15833-2.
[15] J. J. Rehr *et al.,* J. Am. Chem. Soc. **113**, 5135 (1991).
[16] J. Mustre de Leon *et al.,* Phys. Rev. B **44**, 4146 (1991).
[17] M. Baenitz *et al.,* in *Novel Forms of Carbon II,* edited by C. L. Renschler, D. M. Cox, J. J. Poush, Y. Achiba, MRS Symposia Proceedings No. 349 (Material Research Society, Pittsburgh, 1994), p. 301.
[18] M. Baenitz *et al.,* Solid State Commun. **91**, 337 (1994).
[19] H. Werner, Ph.D. thesis, Universität Frankfurt/Main, 1995.
[20] M. Baenitz *et al.,* Physica C **228**, 181 (1994).
[21] W. Bensch *et al.,* unpublished results from site-selective Rietveld analyses; for the K_2CsC_{60} system investigated here, a site selectivity of 95(1)% was found.
[22] M. Kanowski *et al.,* Appl. Magn. Reson. (to be published).
[23] E. D. Crozier, J. J. Rehr, and R. Ingalls, *Chemical Analysis* (John Wiley, New York, 1988), Vol. 92, Chap. 9, p. 373.
[24] *American Institute of Physics Handbook,* third edition (McGraw-Hill, New York, 1972) ISBN 07-001485-X.
[25] G. Nowitzke, Ph.D. thesis, Universität-GH Paderborn, 1994; G. Nowitzke *et al.* (unpublished).
[26] D. Bonnin *et al.,* J. Phys. Colloq. **47**, C8-865 (1986); C. Fretigny *et al., ibid.* **47**, C8-869 (1986).
[27] I. Hirosawa *et al.,* Phys. Rev. B **51**, 3038 (1995).
[28] J. Dumschat, diplom thesis, Universität-GH Paderborn, 1993.
[29] M. Kanowski *et al.,* Appl. Magn. Reson. **8**, 173 (1995).
[30] G. Zimmer *et al.,* Europhys. Lett. **24**, 59 (1993); G. Zimmer *et al.,* in *Electronic Properties of Fullerenes,* edited by H. Kuzmany, J. Fink, M. Mehring, and S. Roth, Springer Series of Solid State Sciences (Springer, Berlin, 1993), Vol. 117, p. 339.